

# PCCP

Accepted Manuscript



This is an *Accepted Manuscript*, which has been through the Royal Society of Chemistry peer review process and has been accepted for publication.

*Accepted Manuscripts* are published online shortly after acceptance, before technical editing, formatting and proof reading. Using this free service, authors can make their results available to the community, in citable form, before we publish the edited article. We will replace this *Accepted Manuscript* with the edited and formatted *Advance Article* as soon as it is available.

You can find more information about *Accepted Manuscripts* in the [Information for Authors](#).

Please note that technical editing may introduce minor changes to the text and/or graphics, which may alter content. The journal's standard [Terms & Conditions](#) and the [Ethical guidelines](#) still apply. In no event shall the Royal Society of Chemistry be held responsible for any errors or omissions in this *Accepted Manuscript* or any consequences arising from the use of any information it contains.

Cite this: DOI: 10.1039/c0xx00000x

www.rsc.org/xxxxxx

## COMMUNICATION

## Nitrogen-doped carbon nanoparticles derived from acrylonitrile plasma for electrochemical oxygen reduction†

Gasidit Panomsuwan,<sup>\*a</sup> Nagahiro Saito<sup>bcd</sup> and Takahiro Ishizaki<sup>ad</sup>

Received (in XXX, XXX) Xth XXXXXXXXX 20XX, Accepted Xth XXXXXXXXX 20XX

DOI: 10.1039/b000000x

Nitrogen-doped carbon nanoparticles were synthesized *via* a solution plasma process, with acrylonitrile as a single-source precursor, followed by a post-thermal annealing process. The nitrogen-bonding states can be tuned by varying the annealing temperature. The best electrocatalytic activity for oxygen reduction reaction (ORR) in terms of both onset potential and limiting current density can be achieved for the catalyst annealed at an optimal temperature of 800 °C because of the high content of graphitic-N catalytic sites and a large specific surface area.

The cathodic oxygen reduction reaction (ORR) plays the most crucial role in controlling overall performance, stability, and reliability of fuel cells.<sup>1</sup> So far, Pt nanoparticles supported on carbon materials (Pt/C) represent the state-of-the-art ORR catalysts as a result of excellent ORR activity (*i.e.*, low overpotential and large current density) and selectivity toward a direct four-electron pathway in both acid and alkaline solutions.<sup>2</sup> However, limited natural resources, high prices, poor long-term durability, and the methanol crossover/carbon monoxide (CO) poisoning effects of Pt are the major hurdles impeding the current development of fuel cells for large-scale commercialization. To address these critical issues, tremendous research efforts have been devoted to developing and exploring alternative Pt-free ORR catalysts to rival Pt/C catalysts in activity and durability.<sup>3–5</sup> Recently, nitrogen-doped carbon materials (*e.g.*, nanoparticles,<sup>6</sup> nanotube,<sup>7</sup> nanocage,<sup>8</sup> graphene,<sup>9</sup> mesoporous,<sup>10</sup> and their composite systems<sup>11,12</sup>) have been considered the most promising candidates as the next generation of low-cost ORR catalysts because they exhibit competitive ORR activity, superior long-term durability, and tolerance to poisoning compared to those of Pt/C catalysts. Density functional theory (DFT) calculations have demonstrated that the incorporation of nitrogen atoms can induce the alteration in atomic charge density and spin density distributions of the nitrogen-doped carbons, thus creating charged sites favorable for the side-on O<sub>2</sub> surface adsorption, which effectively promote the ORR process.<sup>7,13,14</sup>

Over recent years, nitrogen-doped carbon materials have been synthesized from a wide variety of carbon- and nitrogen-source precursors through various strategies, such as chemical vapor deposition,<sup>15</sup> hydrothermal carbonization,<sup>16</sup> plasma treatment,<sup>17</sup> and high-temperature pyrolysis.<sup>18–20</sup> Very recently, plasma in liquid phase, named “solution plasma,” has proven to be an alternative strategy for the synthesis of carbon materials with *in*

*situ* nitrogen doping from a liquid organic precursor containing carbon and nitrogen atoms without the involvement of a metal catalyst.<sup>21,22</sup> This synthetic strategy has paved the way for the synthesis of nitrogen-doped carbon materials using a novel nitrogen-containing liquid precursor. However, owing to an emergent stage of solution plasma process in this field, the precursors for synthesis of nitrogen-doped carbon materials with high yield, nitrogen-rich composition, and good ORR activity level are currently limited, and a more in-depth screening process is greatly required. In this regard, searching for a suitable and low-cost precursor still remains an ongoing challenge in the continuing efforts to develop nitrogen-doped carbon materials synthesized *via* the solution plasma process.

In this communication, we present the synthesis of nitrogen-doped carbon nanoparticles *via* the solution plasma process with acrylonitrile (C<sub>3</sub>H<sub>3</sub>N) as a simple single-source precursor. Briefly, the plasma in liquid acrylonitrile was generated by applying microsecond bipolar high-voltage pulses with a high frequency to a pair of tungsten electrodes (see experimental setup in Fig. S1†). After the plasma was generated, the black soot particles were readily produced from the plasma zone and subsequently ejected into a liquid phase. The reactive species generated by acrylonitrile plasma was monitored *in situ* by optical emission spectroscopy (OES), as shown in Fig. 1. The optical emission spectrum shows the dominant emissions of Swan bands originating from diatomic carbon molecules (C<sub>2</sub>) (transition d<sup>3</sup>Π<sub>g</sub> → a<sup>3</sup>Π<sub>u</sub>; sequences Δ*v* = –2, –1, 0, +1, +2) at the wavelength range of 430–630 nm.<sup>22,23</sup> The emission peaks at 487 and 656 nm are associated with Balmer atomic hydrogen H<sub>β</sub> and H<sub>α</sub>, respectively. Additionally, the strong emission peaks attributing to the CN violet system (transition B<sup>2</sup>Σ<sup>+</sup> → X<sup>2</sup>Σ<sup>+</sup>; sequence Δ*v* = –1, 0, +1) are observed at the shorter wavelengths of 350–420 nm.<sup>24,25</sup> The OES data suggest that acrylonitrile molecules were dissociated into small fragments (*i.e.*, C<sub>2</sub>, CH, H, CN) as the result of high electron and ion temperatures in the plasma zone. These fragments subsequently undergo interaction and recombination processes, leading to the growth and formation of carbon particles with a homogeneous incorporation of nitrogen atoms. As-synthesized catalyst (designated as NCNP) was collected and post-annealed at different temperatures ranging from 500 to 900 °C for 1 h under Ar flow. For simplicity, the annealed catalysts are hereafter designated as NCNP-*T*, where *T* represents the annealing temperature (*i.e.*, 500, 600, 700, 800, and 900 °C).

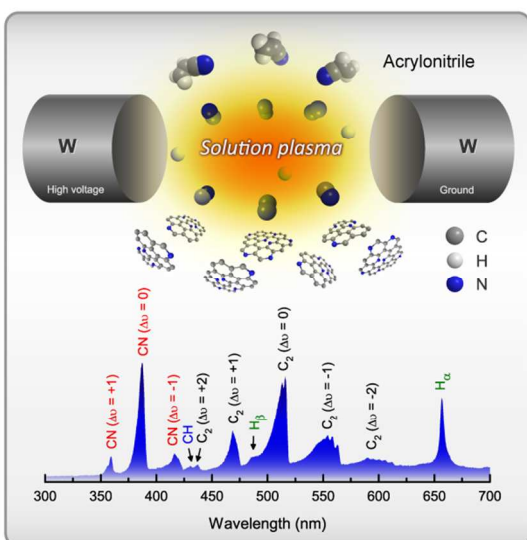


**Fig. 1** Schematic illustration showing the synthesis of nitrogen-doped carbon nanoparticles *via* the solution plasma process and the corresponding optical emission spectrum of plasma generated in liquid acrylonitrile.

The morphology of the catalysts was first investigated by transmission electron microscopy (TEM). A representative bright-field TEM image of NCNP-800 reveals the formation of aggregates of small carbon particles with a diameter of approximately 15–40 nm (Fig. 2a and Fig. S2†). The corresponding selected area electron diffraction (SAED) pattern shows the diffuse diffraction rings (the inset of Fig. 2a), which is the characteristic of turbostratic carbon structure.<sup>26</sup> There is no noticeable change in morphology and particle size with an increase in annealing temperature as observed by TEM images. A high-resolution TEM image of NCNP-800 in Fig. 2b reveals that the carbon particles comprise a mixture of graphitic, turbostratic, and amorphous phases. Energy dispersive spectroscopy (EDS) elemental mapping images of NCNP-800 are shown in Fig. 2c. The carbon, oxygen, and nitrogen elements are evenly distributed throughout the whole area investigated, indicating a homogeneous incorporation of nitrogen atoms into the carbon structure. The specific surface area of all catalysts was determined from nitrogen adsorption data at a relative pressure range of 0.05–0.30 using the Brunauer–Emmett–Teller (BET) method. The specific surface area of annealed catalysts (NCNP-*T*) is found to be in the range of 236–255 m<sup>2</sup> g<sup>-1</sup>, which is much higher than that of NCNP (155 m<sup>2</sup> g<sup>-1</sup>) (Fig. 2d). The higher specific surface area of the annealed catalysts is essential for promoting more accessible catalytic sites for the ORR.<sup>10,27</sup>

The phase structure of the catalysts was further confirmed by X-ray diffraction (XRD). Fig. 3a shows the evolution of a major diffraction peak corresponding to the (002) basal plane of graphite for the catalysts annealed at different temperatures. All XRD patterns show the broad (002) diffraction peaks located at almost the same position ( $2\theta \approx 23.9^\circ$ ) regardless of the change in annealing temperature. The corresponding lattice spacing ( $d_{002}$ ) of all catalysts is calculated to be approximately 0.3722 nm. More structural information was obtained from Raman spectroscopic data. As shown in Fig. 3b, all Raman spectra reveal two evident

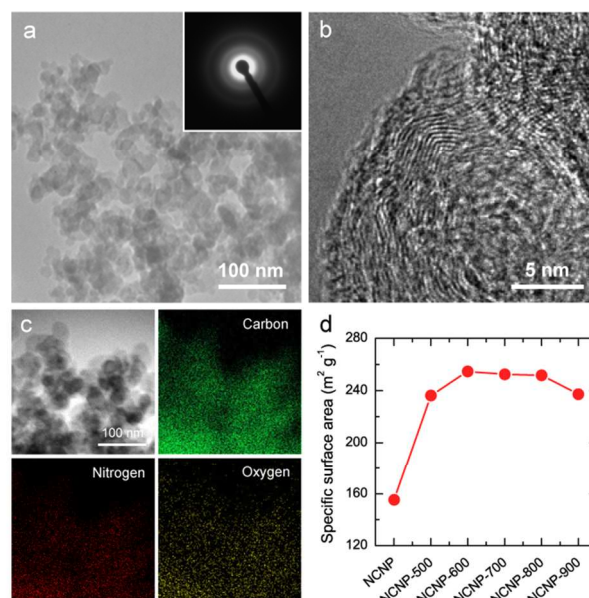


**Fig. 2** (a) Bright-field TEM image of NCNP-800 and the corresponding SAED pattern (inset). (b) High-resolution TEM image of NCNP-800. (c) EDS elemental mapping images of NCNP-800 showing the distribution of carbon, nitrogen, and oxygen elements. (d) Specific surface area of the catalysts annealed at different temperatures.

peaks at approximately 1348 cm<sup>-1</sup> and 1595 cm<sup>-1</sup>, which correspond to the D-band (disordered carbon) and G-band (ordered graphitic carbon), respectively.<sup>28</sup> The relative intensity ratio of the D-band to the G-band ( $I_D/I_G$ ) is found to increase gradually with increasing annealing temperatures from 0.98 for NCNP to 1.04 for NCNP-900. This result may be ascribed to the decomposition of epoxy and hydroxyl groups at high annealing temperatures, leading to the in-plane C=C crack.<sup>29</sup> The results obtained from XRD and Raman spectroscopy suggest that the annealing temperature has a little influence on the change in bulk structural properties of the catalysts.

The nitrogen content in the catalysts was evaluated by CHN elemental analysis (EA). The detected carbon, hydrogen, and nitrogen contents of all catalysts are listed in Table S1†. The nitrogen content decreases from 3.18 to 0.93 wt% with increasing annealing temperatures. X-ray photoelectron spectroscopy (XPS) measurements were further employed to probe the surface

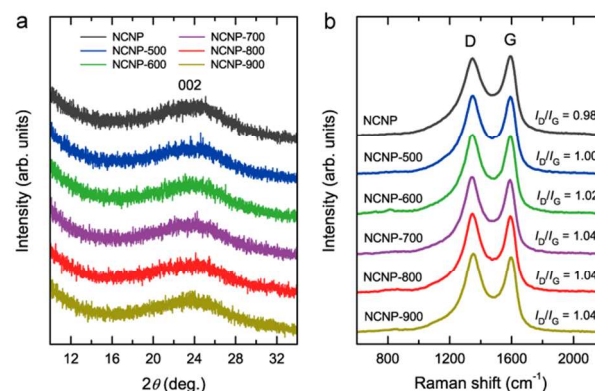


**Fig. 3** (a) XRD patterns and (b) Raman spectra of the catalysts annealed at different temperatures.

elemental composition and chemical bonding states. The XPS survey spectra show the distinct signals of carbon (C 1s), nitrogen (N 1s), and oxygen (O 1s) without any other impurities (Fig. S3†). High-resolution C 1s XPS spectra of all catalysts exhibit the most pronounced peak of graphite-like  $sp^2$  carbon at  $284.5 \pm 0.1$  eV. A tail of asymmetric C 1s peak at higher binding energies is originated from the presence of carbon atoms bonded to nitrogen and different oxygen-containing moieties (Fig. S4a†).<sup>30</sup> The existence of the XPS O 1s peak is most likely due to the oxidation of carbon surface upon exposure to air (Fig. S4b†). Surface elemental compositions of carbon, oxygen, and nitrogen determined from the XPS spectra are listed in Table S1†. An increase in the annealing temperature causes an exponential decrease in the nitrogen content on the catalyst surface from 4.78 at. % for NCNP to 1.33 at. % for NCNP-900 (Fig. 4b), which has a similar tendency with the result obtained from the EA analysis (bulk composition). High-resolution XPS N 1s spectra with deconvolution and peak assignment of the catalysts annealed at different temperatures are shown in Fig. 4a. As can be seen, the XPS N 1s spectral feature evolves from a single peak into a double peak as the annealing temperature increases. This result implies that nitrogen atoms on a catalyst surface are formed by different bonding states depending on the annealing temperature. The XPS N 1s peak of NCNP can be deconvoluted into five components corresponding to pyridinic-N ( $N_p$ :  $398.4 \pm 0.1$  eV), nitrile-N ( $N_N$ :  $399.4 \pm 0.1$  eV), pyrrolic-N ( $N_{PR}$ :  $400.1 \pm 0.2$  eV), graphitic-N ( $N_G$ :  $401.0 \pm 0.1$  eV), and pyridinic N-oxide ( $N_{OX}$ :  $403.7 \pm 0.2$  eV).<sup>31–33</sup> The nitrogen atoms on the surface of NCNP mainly exist in the form of nitrile-N (~62%). When increasing the annealing temperature, the content of nitrile-N and pyrrolic-N substantially decreases, while that of pyridinic-N and graphitic-N progressively increases. The nitrile-N and pyrrolic-N are almost completely decomposed when the annealing temperature increases up to 800 °C. The XPS N 1s peaks of both NCNP-800

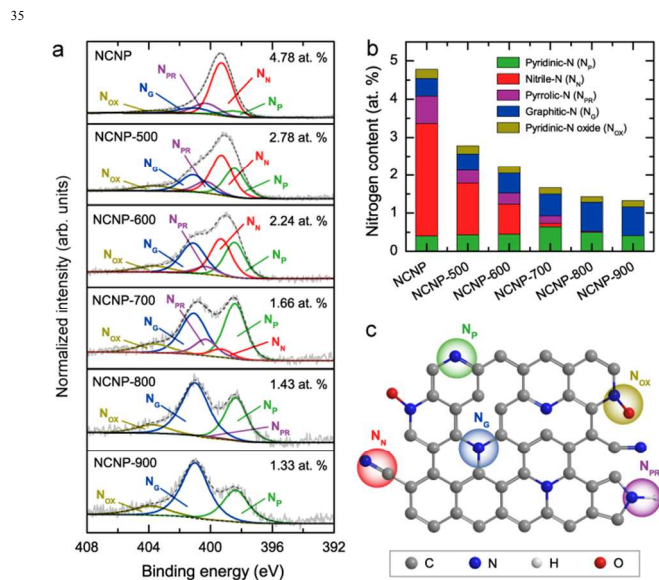


**Fig. 4** (a) High-resolution N 1s XPS spectra with deconvolution and peak assignment of the catalysts annealed at different temperatures. (b) The content of different nitrogen-bonding states for the catalysts annealed at different temperatures. (c) Schematic illustration of various nitrogen-bonding states on the NCNP catalysts.

and NCNP-900 are dominantly composed of pyridinic-N and graphitic-N, with pyridinic-N oxide being the minor component. The content of pyridinic-N reaches a maximum value of 0.64 at. % at 700 °C and decreases at higher temperatures ( $> 700$  °C) as a result of its instability. In the case of graphitic-N, its content continuously increases up to 0.76 at. % at 800 °C and remains nearly stable at temperatures exceeding 800 °C. The content of each nitrogen-bonding state and their relative percentages of the catalysts annealed at different temperatures are summarized in Fig. 4b and Table S3†. This finding indicates that the thermal annealing is an important process in transforming the nitrogen-bonding state from nitrile-N and pyrrolic-N to either pyridinic-N or graphitic-N.

The electrocatalytic activity toward the ORR for all catalysts was investigated with a three-electrode system in a 0.1 M KOH solution at room temperature. The same amount of each catalyst was loaded onto a glassy carbon (GC) rotating disk electrode (RDE) for the electrochemical measurements ( $0.2 \text{ mg}_{\text{cat}} \text{ cm}^{-2}$ ). For comparison, a commercial 20 wt% Pt on Vulcan XC-72 (20% Pt/C) with the same loading was tested as a benchmark. The preparation method of catalyst ink and catalyst-modified GC electrode is given in supplementary information†. Cyclic voltammetry (CV) measurements were first evaluated in both  $N_2$ - and  $O_2$ -saturated 0.1 M KOH solutions at a scan rate of  $50 \text{ mV s}^{-1}$ . The CV curves of all catalysts show a featureless characteristic in  $N_2$ -saturated solution, and the area under the CV curves is quite correlated with the observed specific surface area (Fig. S6†). In  $O_2$ -saturated solution, a well-defined cathodic peak corresponding to the ORR is clearly observed for all CV curves (Fig. 5a and Fig. S6†). To gain deeper insight into the ORR activity, linear sweep voltammetry (LSV) measurements were carried out in an  $O_2$ -saturated 0.1 M KOH solution at a rotation speed of 1600 rpm and a scan rate of  $10 \text{ mV s}^{-1}$ , as shown in Fig. 5b. The LSV curve of NCNP reveals the onset potential for the ORR at  $-0.22$  V with a relatively low limiting current density of  $2.32 \text{ mA cm}^{-2}$  at  $-0.6$  V. After annealing, the onset potential for the ORR significantly shifts to a more positive potential concomitant with a remarkable increase in limiting current density. Among the catalysts studied, NCNP-800 exhibits the most positive onset potential of  $-0.14$  V and the largest current density of  $3.48 \text{ mA cm}^{-2}$  at  $-0.6$  V. There is no further improvement in both the onset potential and limiting current density for NCNP-900. To elucidate the ORR mechanisms and kinetics, the LSV measurements were carried out at different rotation speeds from 225 to 2500 rpm (Fig. 5c and Fig. S7†). Obviously, the limiting current density progressively increases with increasing rotation speed, indicating a shortened diffusion distance at higher rotation speeds.<sup>34</sup> The electron transfer number ( $n$ ) per oxygen molecule in the ORR process can be determined on the basis of the Koutecky–Levich (K–L) equation.<sup>10,35</sup> The K–L plots ( $J^{-1}$  versus  $\omega^{-1/2}$ ) derived from the LSV curves at different rotation speeds exhibit good linearity for all catalysts, and their slopes remain nearly constant over the potential ranges from  $-0.4$  to  $-0.6$  V (Fig. S8†). The  $n$  value of NCNP is calculated to be 2.42 at  $-0.5$  V, suggesting that the ORR process proceeds through a dominant two-electron pathway. The most active NCNP-800 exhibits the highest  $n$  value of 3.15 at  $-0.5$  V among the catalysts studied. This result indicates that the ORR

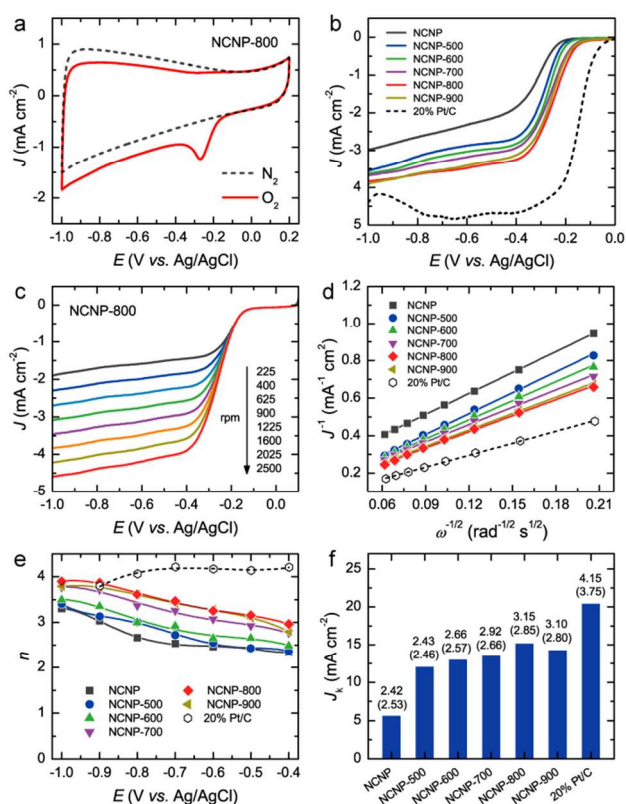


**Fig. 5** Electrochemical measurements: (a) CV curves of the ORR for NCNP-800 in  $N_2$  and  $O_2$ -saturated 0.1 M KOH solutions at a scan rate of  $50 \text{ mV s}^{-1}$  ( $N_2$ : dashed line,  $O_2$ : solid line). (b) LSV curves of the ORR for various catalysts in an  $O_2$ -saturated 0.1 M KOH solution at a rotation speed of 1600 rpm and a scan rate of  $10 \text{ mV s}^{-1}$ . (c) LSV curves of NCNP-800 at different rotation speeds from 225 to 2500 rpm. (d) The corresponding K–L plots of  $J^{-1}$  versus  $\omega^{-1/2}$  of various catalysts at a potential of  $-0.5 \text{ V}$ . (e) Electron transfer number ( $n$ ) of various catalysts in the potentials ranging from  $-0.4$  to  $-1.0 \text{ V}$ . (f) Summary of  $J_k$  and  $n$  values on the basis of the K–L analysis and the RRDE measurements (values in parentheses) of various catalysts at a potential of  $-0.5 \text{ V}$ .

process on NCNP-800 proceeds preferentially *via* parallel two-electron and four-electron pathways, while a four-electron pathway is dominant at higher negative potentials (Fig. 5e). The  $n$  value of 20% Pt/C is approximately 4 over the potential range investigated, confirming a direct four-electron pathway. In addition, the kinetic-limiting current density ( $J_k$ ) also can be determined from the intercept of the linearly fitted K–L plot. The  $J_k$  value of NCNP-800 is  $15.16 \text{ mA cm}^{-2}$  at  $-0.5 \text{ V}$ , which is almost three times greater than that of NCNP ( $5.62 \text{ mA cm}^{-2}$ ) at the same potential. The  $n$  and  $J_k$  values derived from the K–L plots show a similar changing tendency with the ORR activity order (*i.e.*, onset potential and limiting current density) as discussed above. Furthermore, rotating-ring disk electrode (RRDE) measurements were carried out to confirm the reduction pathway derived from the K–L plots. The corresponding  $n$  values can be calculated by monitoring the formation of intermediate peroxide species (*i.e.*,  $HO_2^-$  in alkaline solution) over the catalysts during the ORR process.<sup>36</sup> From the disk and ring currents in Fig. S9† (1600 rpm), the  $HO_2^-$  yield produced by NCNP-800 is calculated to be 42–53%, which is much lower than that produced by NCNP (64–75%) over the whole potential range

from  $-1.0$  to  $-0.3 \text{ V}$  (Fig. S10†). The  $n$  values calculated from the RRDE measurements of all catalysts and 20% Pt/C are consistent with those derived from the K–L plots (Fig. 5f).

We next discuss the factor that plays a role in the improved ORR activity of the catalysts. According to the aforementioned results, the change in annealing temperature leads to a change in specific surface area as well as a significant evolution in both the content and bonding state of nitrogen, while the structural bulk properties are slightly changed. The combination of XPS and electrochemical results demonstrates that the decreased overall nitrogen content with increasing the annealing temperature does not lead to a drop in the ORR activity. This suggests that the ORR activity does not depend on the overall content of nitrogen but rather on how the nitrogen atoms form in the carbon structures. In general, the enhancement in the ORR activity of nitrogen-doped carbon materials is mainly attributed to either pyridinic-N or graphitic-N, while other bonding states seem to have a negligible effect.<sup>37</sup> Specific surface area of the catalysts is also an important factor that should be considered concurrently because the higher surface area can facilitate the exposure of catalytic sites for the ORR.<sup>10,27</sup> Therefore, low ORR activity and small  $n$  values of NCNP are reasonably attributed to a low specific surface area ( $155 \text{ m}^2 \text{ g}^{-1}$ ) and low effective ORR catalytic sites. An enhanced ORR activity of NCNP-500 and NCNP-600 is possibly the results of both larger specific surface area and higher content of pyridinic-N and graphitic-N compared to those of NCNP. With further increases in the annealing temperature (600–800 °C), the specific surface area of the catalysts remains nearly unchanged ( $252$ – $255 \text{ m}^2 \text{ g}^{-1}$ ). This result implies that change in the ORR activity of the catalysts annealed at 600–800 °C predominantly depends on only the type of nitrogen-bonding state. The ORR activity, in terms of both onset potential and limiting current density, continues to increase up to 800 °C even though the content of pyridinic-N decreases at an annealing temperature greater than 700 °C. This result suggests that the pyridinic-N sites may not be the key factor in the improved ORR activity. On the other hand, the improvement of ORR activity seems to be well correlated with the evolution of graphitic-N content. This important finding is evidence that the presence of graphitic-N sites on the catalysts seems to play the dominant role in the improvement of ORR activity in our study, which is in agreement with several previous reports.<sup>10,13,38–40</sup> A slight drop in the ORR activity of NCNP-900 may be caused by a slight decrease in specific surface area compared to that of NCNP-800. Based on the above discussion, the best ORR activity on NCNP-800 can be attributed to the synergistic effect of high graphitic-N content and large surface area at an optimal annealing temperature of 800 °C.

Durability is another important characteristic of the ORR catalysts for practical fuel cell applications. Current–time ( $I$ – $t$ ) chronoamperometric response was performed on NCNP-800 and 20% Pt/C catalysts in an  $O_2$ -saturated 0.1 M KOH solution at a constant potential of  $-0.4 \text{ V}$  with a rotation speed of 1600 rpm for 40000 s to confirm their durability, as shown in Fig. 6a. The relative current of NCNP-800 exhibits a slow attenuation rate with retaining high relative current of 84% after 40000 s. In contrast, the relative current of 20% Pt/C remarkably decreases

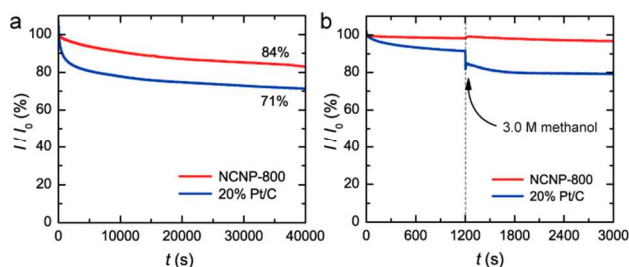


**Fig. 6** (a) Current-time ( $I-t$ ) chronoamperometric response (1600 rpm) of NCNP-800 and 20% Pt/C at  $-0.4$  V in an  $O_2$ -saturated 0.1 M KOH solution for 40000 s. (b) Methanol crossover test of NCNP-800 and 20% Pt/C. The arrow indicates the introduction of 3.0 M methanol.

to 71% after 40000 s. To further assess the tolerance to the methanol crossover effect, 3.0 M methanol was introduced into an  $O_2$ -saturated 0.1 M KOH solution during the measurement of  $I-t$  chronoamperometric response at 1200 s (Fig. 6b). After the introduction of 3.0 M methanol, the current of NCNP-800 is almost unchanged, whereas that of 20% Pt/C greatly drops by approximately 13%. This result confirms that NCNP-800 demonstrates a superior durability and tolerance to the methanol crossover effect in an alkaline solution compared to those of 20% Pt/C. Although the ORR activity of NCNP-800 is not yet as comparable as that of 20% Pt/C, its good ORR activity and reliable stability hold promise for use in direct methanol alkaline fuel cells.

In summary, NCNPs have been successfully synthesized using the solution plasma process with acrylonitrile as a single-source precursor. The annealing temperature has a strong influence in the evolution of nitrogen-bonding states on the catalysts, which significantly affect the ORR activity. The best ORR activity and selectivity of NCNP-800 are mainly attributed to the synergistic effect of a high content of graphitic-N catalytic sites and a large specific surface area at an optimal annealing temperature. Moreover, NCNP-800 exhibits excellent long-term durability and tolerance against methanol crossover effect compared to those of 20% Pt/C. Our finding in this study not only has added acrylonitrile as a suitable precursor for the synthesis of nitrogen-doped carbons *via* the solution plasma process but also provides the important role of an annealing temperature for realizing a high ORR activity level.

## Notes and references

<sup>a</sup>Department of Materials Science and Engineering, Faculty of Engineering, Shibaura Institute of Technology, Tokyo 135-8548, Japan. E-mail: i036050@sic.shibaura-it.ac.jp, g.panomsuwan@gmail.com Fax: +81-3-5859-8101; Tel: +81-3-5859-8115

<sup>b</sup>Department of Materials, Physics and Energy Engineering, Graduate School of Engineering, Nagoya University, Nagoya 464-8603, Japan.

<sup>c</sup>Green Mobility Collaborative Research Center, Nagoya University, Nagoya 464-8603, Japan.

<sup>d</sup>Core Research for Evolutional Science and Technology (CREST), Japan Science and Technology Agency (JST), Saitama 333-001, Japan.

† Electronic Supplementary Information (ESI) available: Experimental section, characterizations, electrochemical measurements, particle size distribution of NCNP-800, XPS survey spectra, high-resolution XPS C 1s, O 1s and N 1s spectra with deconvolution, CV curves in  $N_2$  and  $O_2$ -saturated 0.1 M KOH, LSV curves at different rotation speeds, the K-L plots, RRDE measurement,  $n$  and  $J_k$  derived from the RRDE measurement as a function of potential, comparative CV curves of

NCNP-800 and 20% Pt/C with and without 3.0 M methanol. See DOI: 10.1039/b000000x/

- 1 Y. Qiao, S.-J. Bao and C. M. Li, *Energy Environ. Sci.*, 2010, **3**, 544.
- 2 X. Zhao, M. Yin, L. Ma, L. Liang, C. Liu, J. Liao, T. Lu and W. Xing, *Energy Environ. Sci.*, 2011, **4**, 2736.
- 3 A. Morozan, B. Jousselme and S. Palacin, *Energy Environ. Sci.*, 2011, **4**, 1238.
- 4 G. Wu and P. Zelenay, *Acc. Chem. Res.*, 2013, **46**, 1878.
- 5 N. Daem, X. Sheng, I. F. J. Vakelecom and P. P. Pesscarmona, *J. Mater. Chem. A*, 2014, **2**, 4085.
- 6 T. Xing, J. Sunarso, W. Yang, Y. Yin, A. M. Glushenkov, L. H. Li, P. C. Howlett and Y. Chen, *Nanoscale*, 2013, **5**, 7670.
- 7 K. Gong, F. Du, Z. Xia, M. Durstock and L. Dai, *Science*, 2009, **323**, 760.
- 8 S. Chen, J. Bi, Y. Zhao, L. Yang, C. Zhang, Y. Ma, Q. Wu, Z. Wang and Z. Hu, *Adv. Mater.*, 2012, **24**, 5593.
- 9 C. Zhu and S. Dong, *Nanoscale*, 2013, **5**, 1753.
- 10 R. Liu, D. Wu, X. Feng and K. Müllen, *Angew. Chem. Int. Ed.*, 2010, **49**, 2565.
- 11 X. Zhou, Z. Tian, J. Li, H. Ruan, Y. Ma, Z. Yang and Y. Qu, *Nanoscale*, 2014, **6**, 2603.
- 12 H. T. Chung, J. H. Won and P. Zeleney, *Nat. Commun.*, 2013, **4**, 1922.
- 13 H. Kim, K. Lee, S. I. Woo and Y. Jung, *Phys. Chem. Chem. Phys.*, 2011, **13**, 17505.
- 14 L. Zhang, Z. Xia, *J. Phys. Chem. C*, 2011, **115**, 11170.
- 15 Z. Chen, D. Huggins, H. Tao, R. S. Hsu and Z. Chen, *J. Phys. Chem. C*, 2009, **113**, 21008.
- 16 S.-A. Wohlgemuth, T.-P. Fellingner, P. Jäker and M. Antonietti, *J. Mater. Chem. A*, 2013, **1**, 4002.
- 17 Y. Shao, S. Zhang, M. H. Engelhard, G. Li, G. Shao, Y. Wang, J. Liu, I. A. Aksay and Y. Lin, *J. Mater. Chem.*, 2010, **20**, 7491.
- 18 Z.-H. Sheng, L. Shao, J.-J. Chen, W.-J. Bao, F.-B. Wang and X.-H. Xia, *ACS Nano*, 2011, **5**, 4350.
- 19 Z. Lin, G. Waller, Y. Liu, M. Liu and C.-P. Wong, *Adv. Energy Mater.*, 2012, **2**, 884.
- 20 C. Cao, X. Zhaung, Y. Su, Y. Zhang, F. Zhang, D. Wu and X. Feng, *Polym. Chem.*, 2014, **5**, 2057.
- 21 G. Panomsuwan, S. Chiba, Y. Kaneko, N. Saito and T. Ishizaki, *J. Mater. Chem. A*, 2014, **2**, 18677.
- 22 D.-W. Kim, O. L. Li and N. Saito, *Phys. Chem. Chem. Phys.*, 2015, **17**, 407.
- 23 S. S. Harilal, R. C. Issac, C. V. Bindhu, V. P. N. Nampoori and C. P. G. Vallabhan, *J. Phys. D: Appl. Phys.*, 1997, **30**, 1703.
- 24 S. F. Durrant, E. C. Rangel and M. A. Bica de Moraes, *J. Vac. Sci. Technol. A*, 1995, **13**, 1901.
- 25 A. E. Lefohn, N. M. Mackie and E. R. Fisher, *Plasmas Polym.*, 1998, **3**, 197.
- 26 H. Hou, J. J. Ge, J. Zeng, Q. Li, D. H. Reneker, A. Greiner and S. Z. D. Cheng, *Chem. Mater.*, 2005, **17**, 967.
- 27 H.-W. Liang, W. Wei, Z.-S. Wu, X. Feng and K. Müllen, *J. Am. Chem. Soc.*, 2013, **135**, 16002.
- 28 M. S. Dresselhaus, A. Jorio, M. Hofmann, G. Dresselhaus, R. Saito, *Nano Lett.*, 2010, **10**, 751.
- 29 Z. Lin, G. H. Waller, Y. Liu, M. Liu and C.-P. Wong, *Carbon*, 2013, **53**, 130.
- 30 A. Valázquez-Palenzuela, L. Zhang, L. Wnag, P. L. Cabot, E. Brillias, K. Tsay and J. Zhang, *J. Phys. Chem. C*, 2011, **115**, 12929.
- 31 J. R. Pels, F. Kapteijn, J. A. Moulijn, Q. Zhu and K. M. Thomas, *Carbon*, 1995, **33**, 1641.
- 32 F. Jaouen, J. Herranz, M. Lefèvre, J.-P. Dodelet, U. I. Kramm, I. Herrmann, P. Bogdanoff, J. Maruyama, T. Nagaoka, A. Garsuch, J. R. Dahn, T. Olson, S. Pylypenko, P. Atanassov and E. A. Ustinov, *ACS Appl. Mater. Interf.*, 2009, **1**, 1623.
- 33 W. Ding, Z. Wei, S. Chen, X. Qi, T. Yang, J. Hu, D. Wang, L.-J. Wan, S. F. Alvi and L. Li, *Angew. Chem. Int. Ed.*, 2013, **52**, 11755.
- 34 L. Qu, Y. Liu, J.-B. Baek and L. Dai, *ACS Nano*, 2010, **4**, 1321.
- 35 S. Treimer, A. Tang and D. C. Johnson, *Electroanal.*, 2002, **14**, 165.
- 36 K. Ke, T. Hatanaka and Y. Morimoto, *Electrochim. Acta*, 2011, **56**, 2098.

- 
- 37 L. Lai, J. R. Potts, D. Zhan, L. Wang, C. K. Poh, C. Tang, H. Gong, Z. Shen, J. Lin and R. S. Ruoff, *Energy Environ. Sci.*, 2012, **5**, 7936.
- 38 Z. Q. Luo, S. H. Lim, Z. Q. Tian, J. Z. Shang, L. F. Lai, B. MacDonald, C. Fu, Z. X. Shen, T. Yu and J. Y. Lin, *J. Mater. Chem.*, 2011, **21**, 8038.
- 5 39 D. Geng, Y. Chen, Y. Chen, Y. Li, R. Li, X. Sun, S. Ye and S. Knight, *Energy Environ. Sci.*, 2011, **4**, 760.
- 40 L. Zhang, Z. Su, F. Jiang, L. Yang, J. Qian, Y. Zhou, W. Li and M. Hong, *Nanoscale*, **2014**, **6**, 6590.